




Effect of a subnanometer thin insulator layer at the Ag/Si(111) interface through the observation of quantum well states

R. Flammini ^{1,*}, S. Colonna,¹ P. M. Sheverdyeva,² M. Papagno,³ A. K. Kundu ⁴ and P. Moras ²

¹*CNR-ISM, Istituto di Struttura della Materia, Via del Fosso del Cavaliere 100, I-00133 Roma, Italy*

²*CNR-ISM, Istituto di Struttura della Materia, S.S. 14, km 163.5, I-34149 Trieste, Italy*

³*Dipartimento di Fisica, Università della Calabria, Via P. Bucci, I-87036 Arcavacata di Rende (CS), Italy*

⁴*International Center for Theoretical Physics (ICTP), I-34014 Trieste, Italy*



(Received 18 April 2021; accepted 10 August 2021; published 30 August 2021)

The “two-step” growth technique has been used to grow atomically uniform Ag films on 7×7 Si(111) and 8×8 β -Si₃N₄(0001)/Si(111) surfaces. Angle-resolved photoemission spectroscopy reveals the formation of *sp* quantum well states in the Ag films with distinct properties in the two cases. It is shown that the valence electrons in silver can be confined in the fundamental gap of a less than 1-nm-thin nitride layer, effectively decoupling the Ag and Si states.

DOI: [10.1103/PhysRevMaterials.5.084604](https://doi.org/10.1103/PhysRevMaterials.5.084604)

I. INTRODUCTION

The metal/silicon interface is at the root of all electronic devices. Since the 1940’s with the advent of the transistor [1] until today, with silicon-based solar cells [2], a huge effort has been devoted to optimize the atomic and electronic structure of such a junction. The difference in the band structure between the metal and the semiconductor when put in contact induces a number of interesting effects. As a matter of fact, the Fermi levels must align and, due to the difference in the work function/chemical potential, band bending occurs [3]. One of the consequences is the appearance of metal-induced gap states (MIGS) [4] due to the tail of the electron wave functions of the metal extending into the gap of the silicon. Other kinds of interface states have been observed: trap states (induced by atomic defects in the semiconductor) or, more generally, disorder-induced gap states (DIGS) [5]. However, one of the major issues is represented by a metal/silicon chemical reaction. Indeed, the resulting electronic band structure can also show defect gap states owing to the formation of silicides. The presence of states in the gap can induce Fermi-level pinning, hampering the precise tuning of the Schottky barrier and degrading the performance of the device [6]. An open problem in this context is, for instance, the construction of suitable electrical contacts for solar cells and spintronics devices [7,8]. This is why the idea to passivate the silicon surface before metal deposition has always drawn great attention and it still does nowadays [9].

Regardless of the well-known characteristics of silicon nitride in its amorphous phase [10], with the first studies of the effect of ammonia on a Si(111) surface, evidence for the formation of a thin and ordered nitride layer has indeed been provided. By dosing ammonia at a high temperature, a self-terminating reaction takes place, inducing the formation

of a double layer of β -Si₃N₄(0001) which almost perfectly matches the Si(111) lattice [11,12]. The nitride layer exhibits an 8×8 reconstructed surface, although its surface and interfacial atomic structures are still debated [11,13].

It has been also shown that below the Fermi level no interface or surface states exist, while the nitride layer features an electronlike resonance [14]. The nitride surface is inert against oxidation [15] and acts as a perfect barrier to several metal elements such as gold [16], iron [17,18], cobalt [19,20], or aluminum [21] even at higher temperatures. Indeed, less than 1 nm of such a nitride layer prevents the formation of silicides on a macroscopic scale up to 300 °C [20,22]. The interface with graphene has also been reported in relation to the possibility to use the thin nitride layer as a gate dielectric below 50 K [23]. However, most importantly, no Fermi-level pinning is present at the metal/thin β -silicon nitride/silicon interface [24].

Owing to the two-step growth procedure [25,26], we have been able to create a flat Ag film on the nitride surface, in contrast with the known Volmer-Weber growth mode occurring at room temperature (RT) [16–21,27]. This has made it possible to investigate the role of a buried nitride layer through the observation of quantum well (QW) states of the metallic adsorbate. It is shown that, in contrast to the Ag/Si(111) case, where a subnanometer nitride interlayer is present, the electrons in the silver layer can be fully confined in the nitride gap. This study can be relevant to all cases aiming at reaching ideal (electronically) and sharp (atomically) metal/silicon junctions, where the presence of interface states or a strong band bending are relevant issues.

II. EXPERIMENT

Si(111) samples were cut from *n*-type (P-doped) silicon wafers with resistivity $\rho \simeq 0.005 \Omega \text{ cm}$. The surface was outgassed at 700 K for a few hours. The sample was then cleaned by repeated flashes of several seconds at 1520 K at a base

*roberto.flammini@cnr.it

pressure of $\sim 3 \times 10^{-10}$ mbar, leading to a sharp 7×7 low-energy electron diffraction (LEED) pattern. The 7×7 reconstructed surface was held at a temperature of approximately 1050 K and exposed to 10^2 L (10^{-6} Torr s) of NH_3 . This ensures the growth of two bilayers of silicon nitride [12].

Silicon nitride in the β phase features a hexagonal-close-packed (hcp) lattice structure. The in-plane and out-of-plane lattice constants are $a = b = 7.604$ Å and $c = 2.906$ Å [28], respectively. Silicon displays a face-centered-cubic (fcc) diamond structure with a lattice parameter $a = 5.43$ Å. Hence, both $\beta\text{-Si}_3\text{N}_4(0001)$ and $\text{Si}(111)$ feature a hexagonal surface Brillouin zone (SBZ), although the stacking sequence of the bulk atomic layers is different. For the $\beta\text{-Si}_3\text{N}_4(0001)$, the crystallographic directions and the sizes of $\bar{\Gamma}\bar{K}$ and $\bar{\Gamma}\bar{M}$ are $\langle 10\bar{1}0 \rangle 0.55$ Å $^{-1}$ and $\langle 11\bar{2}0 \rangle 0.48$ Å $^{-1}$, respectively. As for the $\text{Si}(111)$ substrate, the size of the SBZ is almost twice that of the silicon nitride [14].

Silver was deposited by an effusion cell calibrated by a quartz microbalance. We employed the two-step procedure consisting of adsorbate growth at low temperature (less than 100 K) to avoid surface migration and then a slow recovery up to RT to favor adsorbate ordering [29]. The same sample is then flashed again to restore the 7×7 reconstruction and a similar amount of silver has been deposited to allow a reliable comparison with the case of the 8×8 reconstructed surface. We used the monatomic step of $\text{Ag}(111)$ of 2.36 Å as the step height of 1 ML (monolayer) of $\text{Ag}/\text{Si}(111)$.

Angle-resolved photoemission spectroscopy (ARPES) maps were recorded at the VUV-Photoemission Beamline (Elettra, Italy). The spectra were acquired at RT, with photon energies of 40 and 51 eV, for the 7×7 and 8×8 reconstructed surfaces, respectively, using a Scienta R-4000 electron analyzer. Typical total energy and angular resolutions were set to 30 meV (40 eV photon energy) and 0.3° , respectively. The second derivative of the spectroscopy maps has been computed along the energy axis. The Fermi level of the bare surface was measured exploiting the metallicity of the 7×7 reconstructed surface [30].

III. RESULTS

Our study starts from the analysis of the second derivative ARPES maps taken on the 7×7 and 8×8 reconstructed surfaces shown in Figs. 1(a) and 1(b), respectively. Pristine spectra are shown in Figs. S1 and S2 of the Supplemental Material (SM) [31]. Figure 1(a) features the spectra along the $\bar{\Gamma}\text{-}\bar{K}_{\text{Si}}$ high-symmetry direction, taken at a photon energy of 40 eV. From the top of the bulk valence band, at about 0.8 eV below the Fermi level, three bands (holelike) dispersing downwards from $\bar{\Gamma}$ to \bar{K}_{Si} can be assigned to the well-known heavy-hole, light-hole, and split-off bands (labeled HH, LH, and SO). Beside the bulk bands, the S_1 surface state is identified, and is generally attributed to the surface adatoms [30]. This feature is considered to be a signature of the 7×7 reconstruction (see Ref. [32] and references therein).

In Fig. 1(b) we show the electronic band structure of the 8×8 surface, along the $\bar{K}_\beta\bar{\Gamma}\bar{K}_\beta$ high-symmetry direction and recorded at 51 eV photon energy. The three holelike bands originating at $\bar{\Gamma}$ at about 0.7 eV, already seen in Fig. 1(a), are present also in Fig. 1(b). An electronlike band is also

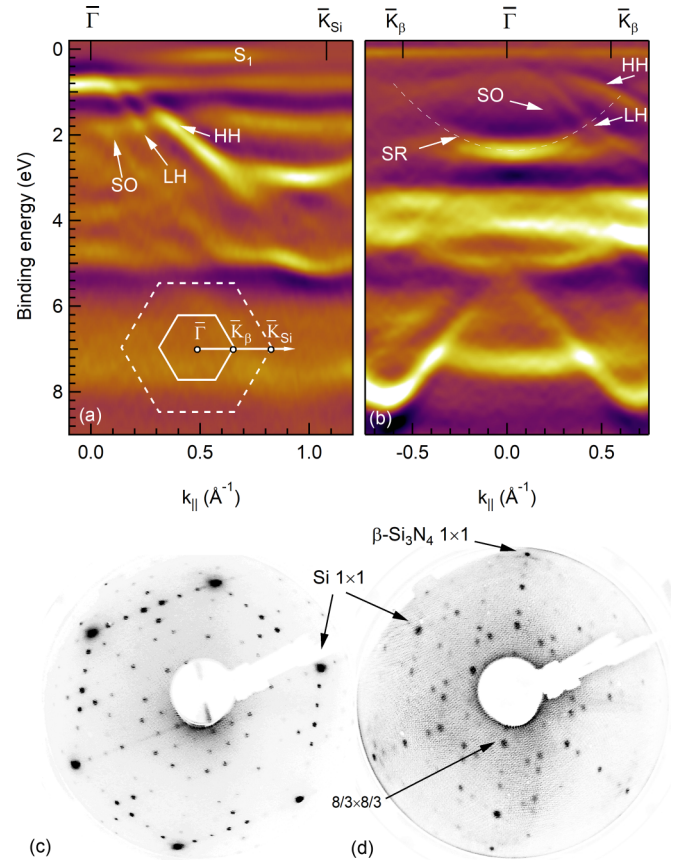


FIG. 1. Second derivative ARPES maps of (a) $\text{Si}(111)\text{-}7 \times 7$ and (b) $\beta\text{-Si}_3\text{N}_4(0001)\text{-}8 \times 8$. The labels HH, LH, and SO mark the heavy-hole, light-hole, and split-off bulk bands, respectively. S_1 and SR indicate the surface and resonant states, respectively. At the bottom of (a), the Brillouin zones and the high-symmetry direction of the ARPES maps are sketched. (c) and (d) display LEED patterns taken on the 7×7 and 8×8 reconstructed surfaces, with 59 and 70 eV primary electron energy, respectively.

noticed, whose minimum lies at about 2.5 eV binding energy, in correspondence of $\bar{\Gamma}$. This parabolic band, labeled SR (surface resonance), is attributed to the presence of the nitride layer [14,15]. The SR overlaps with the silicon (surface projected) bulk bands but no hybridization gap is observed at the band crossing and therefore cannot be ascribed to nitride/silicon mixed states. This is in agreement with the assignment of the band to the topmost atoms of the nitride surface made in the literature [14,15]. The quality of the interface is demonstrated by the rich band structure measured down to 9 eV binding energy. The intensity detected at the Fermi level is attributed to an artifact of the second derivative spectra (see Fig. S2 of SM for comparison).

The choice of 51 eV photon energy is dictated by the maximum in the cross section of the silver Shockley state [33], as will be clear in the following. The quality of the two reconstructed surfaces is also proven by the LEED patterns displayed in Figs. 1(c) and 1(d), in agreement with the literature [34,35].

Figure 2 features ARPES maps along the $\bar{K}_{\text{Si}}\bar{\Gamma}\bar{K}_{\text{Si}}$ direction of silicon upon silver growth on 7×7 and 8×8

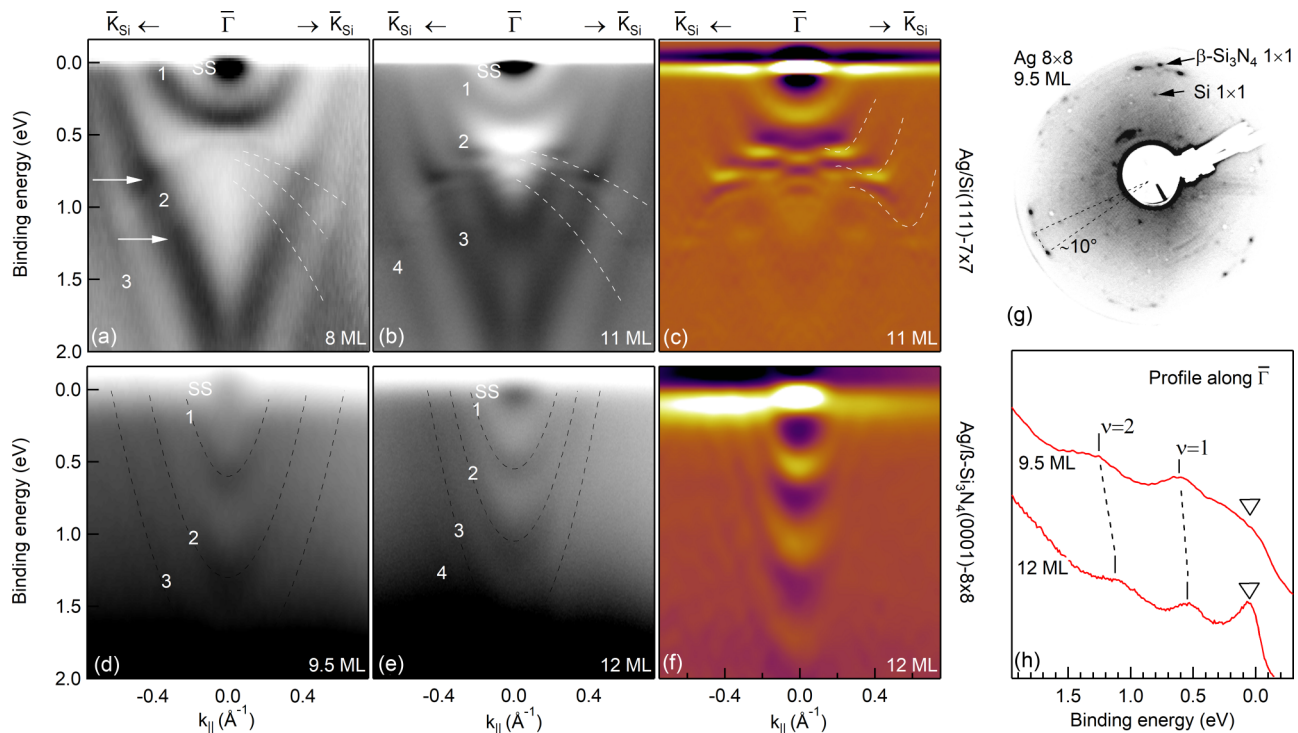


FIG. 2. The top (bottom) panels show the ARPES maps recorded on the 7×7 (8×8) reconstructed surfaces upon silver growth. (a), (b), (d), and (e) display ARPES spectra (as measured), along the $\bar{\Gamma}\bar{K}$ direction, taken at 51 eV photon energy. Darker colors correspond to higher intensity. (c) and (f) feature the second derivative spectra of (b) and (e), respectively. (h) shows profiles taken at $\bar{\Gamma}$ on the images of (d) and (e). The bars and the triangles indicate the QW states and the Shockley surface states, respectively. The LEED pattern taken after the growth of 9.5 ML of silver on the 8×8 reconstructed surface is depicted in (g).

reconstructed surfaces, top and bottom panels, respectively. Figures 2(a), 2(b), 2(d), and 2(e) show the spectra as measured (darker gray corresponds to higher intensity) for different amounts of adsorbate, while Figs. 2(c) and 2(f) show the second derivative images of Figs. 2(b) and 2(e), respectively, to highlight the notable features. In Fig. 2(a) we show the image taken after growth of an 8-ML Ag film. A high image contrast is needed to highlight the presence of faint structures otherwise not visible. Apart from the Shockley surface state (SS) [36], we can see at least three QW states labeled 1–3. At about 0.8 and 1.3 eV binding energy, two areas with higher intensity are noticed, where the bands slightly depart from the parabolic dispersion (white arrows). These kinks are attributed to the hybridization between the Ag QW states and the upper edges (white dashed lines) of the bulk silicon HH, LH, and SO bands, first reported for the Al/Si interface [37]. This explains also why the topmost QW state is nearly parabolic, not suffering the effect of the silicon bulk bands.

In Fig. 2(b) we increased the Ag thickness up to 11 ML and detected a sharper SS and a higher number of QW states, labeled 1–4, where the topmost state is located again above the silicon bulk bands, as in Fig. 2(a). We estimated the amount of silver by comparison with the work of Speer *et al.* [38]. In the binding energy range between 0.5 and 1 eV, we observe fine structures in correspondence with the kinks [more visible in Fig. 2(c)]: These features have been attributed to interference fringes. On this system, the fringe structures have been reported for the first time by Speer *et al.* [38] and arise when a continuous metallic layer, grown on a heavily n -doped silicon

substrate, induces a band bending. The slowly varying potential in the semiconductor allows quantized close-lying levels to interfere with each other, giving rise to the fringe structures. As a matter of fact, the fringe structures are described by Airy functions, solutions of the Schrödinger equation in the case of a potential well in which one of the two walls shows a linearly varying behavior [39]. Therefore, the electrons lying in such energy levels are only partially confined as they cross the bulk bands, resonating with the silicon bulk states [40]. In this respect, it is noticed that the topmost QW state is energetically located above the bulk silicon bands, that is, in the silicon gap, so that the electrons are fully confined by vertical potentials, resulting in a nearly perfect parabolic energy dispersion.

Figures 2(d) and 2(e) show the maps taken on the nitrated surface after deposition of about 9.5 and 12 ML Ag, respectively. The amount of silver has been estimated by the comparison with studies on quantum wells where the silicon surface is passivated [41,42], to rule out the possible effects of lattice strain [29]. The three QWs of Fig. 2(e) show a parabolic dispersion, with an almost identical electron effective mass. The extracted value of $0.58m_e$ is slightly above the range of values (0.38 – 0.50) m_e reported in Ref. [41] for the H-passivated silicon surface, and in agreement with the case of another inert surface such as that of MoS₂, where the authors report a value of $0.5m_e$ [43]. In the case of a Ga-passivated Si(111) surface, Starfelt *et al.* [42] separated the contribution to the effective mass of the resonant from the nonresonant part of the silver quantum wells. Our value is lower than the one expected from the fully confined case. It is likely that

in our case the interaction of the silver film with the nitride surface is weaker than in the case of other passivated silicon surfaces. Furthermore, the bands do not show any deviation from parabolic dispersion even for larger k_{\parallel} , demonstrating that the confining potential does not allow any transmission of the wave functions via possible hybridized states [44]. When comparing the top and bottom ARPES panels of Fig. 2 the absence of the silicon valence states can be noticed. This is due to the short photoelectron escape depth [45].

In this study, we observed also a lack of QWs for less than 8 ML of deposited silver. This could be compatible with an “electronic growth” [28,46], according to which a stabilization of flat and uniform layers is predicted to occur for thicknesses larger than 6 ML on Si(111)- 7×7 [25]. In our case, even if charge spilling is not present [28], quantum confinement and Friedel oscillations may play an important role. Further measurements are planned to investigate the behavior of the QW for different coverage and photon energies.

Figure 2(h) features two energy distribution curves taken at the $\bar{\Gamma}$ point of the spectroscopy maps shown in Figs. 2(d) and 2(e). The QW states shift towards higher binding energies as a function of the amount of adsorbate (as expected from the phase accumulation model [47]), in perfect agreement with Arranz *et al.* [41]. Moreover, the thicker the film, the sharper is the silver surface state. The sharpness of the SS peak and of the QW states also reflects an increased continuity and an improved crystallinity of the film [42]. When comparing the top and bottom panels of Fig. 2, however, a delay in the formation of the surface states is noticed: On the 7×7 the SS is already strong at 8 ML, while barely visible on the 8×8 at 9.5 ML. The larger tensile strain suffered by silver on the nitride surface with respect to the bare silicon surface can explain the depopulation of the SS [29]. However, no strained Ag phase has been recorded by LEED, likely due to the size of the islands being much shorter than the lateral coherence length of the instrument.

No evidence of the SR has been detected in the 1.5–2.5 eV binding energy range (not shown). This can be rationalized by considering that such resonance is due to the topmost atoms of the nitride surface and can also be affected by the interaction with an adsorbate [15] and could possibly disappear. We recorded only the quantum well signature of a flat silver layer, regardless of the low amount of adsorbate. All singularities generally observed through the phase shift at the substrate band edges (as the interaction of the SS and QWs) have not been observed [48], corroborating the interpretation of a full electron confinement only normal to the surface.

In Fig. 2(g) we show the LEED pattern taken after deposition of 9.5 ML of Ag, at the same primary electron energy of the 8×8 surface (70 eV). Apart from the presence of the 1×1 spots, the image still shows the presence of the 8×8 reconstruction (mainly around the electron gun). This is ascribed to the lack of continuity of the silver layer as also known for the 7×7 [25]. A couple of spots rotated by about 10° (and whose lattice vectors are about 22% longer than the 1×1 spots) are also recorded. These rotated triangular domains absent on the bare nitride surface could be related to slightly rotated silver domains. However, on the bare nitride surface, such LEED spots are generally attributed to a degraded nitridation either operating at higher temperatures

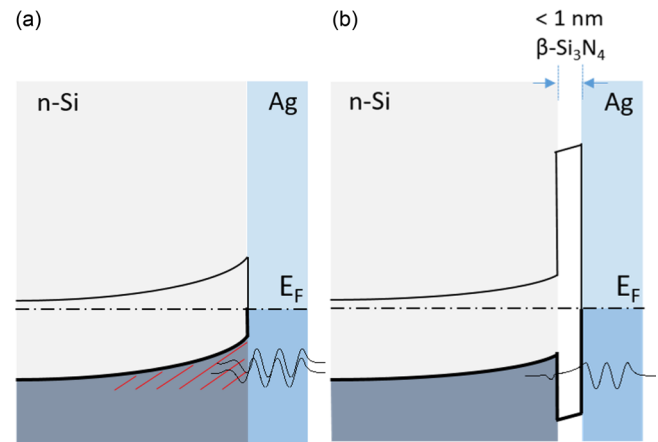


FIG. 3. Sketch of the energy band structure of the highly n (P)-doped Si/Ag interface (a) before and (b) after insertion of the thin silicon nitride layer. Filled states are represented by darker colors. The dashed area features the depletion layer. The black oscillating curves represent the electron wave functions, to guide the eye. The picture is not to scale.

(more than 1300 K) [34,35] or to the presence of carbon contaminants [21] (absent in our case). To our knowledge, a final word on the possible epitaxial growth of the silver cannot be stated.

In Figs. 3(a) and 3(b), we provide a schematic of the energy band structure for silver on silicon and on silicon nitride in thermal equilibrium, respectively. The alignment of the Fermi levels and gap values have been taken from the literature [49,50]. In the case of the Ag/Si interface, a band bending occurs, and the fringe structures form as the electron wave function shows an oscillating tail within the semiconductor bulk projected bands (red dashed area). When the nitride layer is placed in between, the bands only weakly bend, as there is no longer a depletion zone. Moreover, no pinning of the Fermi level occurs (caused by metal silicides or from trap states) and the bending mainly depends on the amount of fixed charges at the β -Si₃N₄/Si interface [24]. However, owing to the thinness of the nitride layer (about 0.6 nm [12]) and to the electron coherence length which can reach dozens of Å [38], the electron wave functions might extend beyond the nitride wall. Therefore, even if the QW energy levels are compatible with a hybridization with the silicon bulk bands (for a binding energy range larger than 0.7 eV), the corresponding electron wave functions, after suffering an attenuation across the nitride layer, cannot interfere with each other because of the strongly reduced band bending. In other words, the QWs observed indicate that the potential barriers confining the electrons in silver can be considered as vertical on both (vacuum and nitride) sides, simulating the case of a nearly free-standing Ag film.

We demonstrate in this study that a thin nitride layer can preserve and keep separated the electronic structures of both the semiconductor substrate and metallic adsorbate. In this respect, large-scale ordered metallic overlayers (with well-defined electronic and magnetic structures), grown on such a thin nitride layer, may contribute to the realization of

spintronics devices: QWs made of magnetic layers, might be useful for the injection of polarized electrons in silicon [51].

IV. CONCLUSION

We have observed quantum well states on the Ag/Si(111) and Ag/ β -Si₃N₄/Si(111) interfaces, by angle-resolved photoemission spectroscopy. This has been made it possible by the two-step growth technique, where silver is first deposited at low temperature and then is left recovering RT. The data display the full confinement of the electrons in the nitride gap for the Ag/ β -Si₃N₄/Si(111) interface, at variance with the case of Ag/Si(111), where the QW states partially resonate with

the continuum of the bulk silicon bands. Therefore, the nitride layer, although very thin (less than 1 nm), restores the vertical potential wall towards the highly *n*-doped silicon substrate, so that silver can show the valence electronic structure of a nearly free-standing layer.

ACKNOWLEDGMENTS

The authors are grateful to Dr. S. Heun for several discussions. A.K.K. acknowledges support from the receipt of a fellowship from the ICTP-TRIL Programme, Trieste, Italy. Technical support from Fabio Zuccaro is acknowledged. We acknowledge the project EUROFEL-ROADMAP ESFRI of the Italian Ministry of Education, University, and Research.

-
- [1] J. Bardeen and W. H. Brattain, *Phys. Rev.* **74**, 230 (1948).
- [2] C. Battaglia, A. Cuevas, and S. De Wolf, *Energy Environ. Sci.* **9**, 1552 (2016).
- [3] H. Lüth, *Solid Surfaces, Interfaces and Thin Films* (Springer, Berlin, 2010).
- [4] J. Tersoff, *Phys. Rev. Lett.* **52**, 465 (1984).
- [5] H. Hasegawa and H. Ohno, *J. Vac. Sci. Technol. B* **4**, 1130 (1986).
- [6] W. Mönch, *Semiconductor Surfaces and Interfaces*, Springer Series in Surface Sciences (Springer, Berlin, 2013).
- [7] F. Léonard and A. A. Talin, *Nat. Nanotechnol.* **6**, 773 (2011).
- [8] R. Jansen, *Nat. Mater.* **11**, 400 (2012).
- [9] L. Black, B. van de Loo, B. Macco, J. Melskens, W. Berghuis, and W. Kessels, *Sol. Energy Mater. Sol. Cells* **188**, 182 (2018).
- [10] X. Meng, Y.-C. Byun, H. S. Kim, J. S. Lee, A. T. Lucero, L. Cheng, and J. Kim, *Materials* **9**, 1007 (2016).
- [11] H. Ahn, C.-L. Wu, S. Gwo, C. M. Wei, and Y. C. Chou, *Phys. Rev. Lett.* **86**, 2818 (2001).
- [12] J. W. Kim and H. W. Yeom, *Phys. Rev. B* **67**, 035304 (2003).
- [13] X.-s. Wang, G. Zhai, J. Yang, and N. Cue, *Phys. Rev. B* **60**, R2146 (1999).
- [14] R. Flammini, P. Allegrini, F. Wiame, R. Belkhou, F. Ronci, S. Colonna, D. M. Trucchi, F. Filippone, S. K. Mahatha, P. M. Sheverdyaeva, and P. Moras, *Phys. Rev. B* **91**, 075303 (2015).
- [15] R. Flammini, A. Bellucci, F. Wiame, R. Belkhou, M. Carbone, D. Trucchi, S. Colonna, F. Ronci, M. Hajlaoui, M. Silly, and F. Sirotti, *Appl. Surf. Sci.* **355**, 93 (2015).
- [16] R. Flammini, F. Wiame, R. Belkhou, M. Marsi, L. Gregoratti, A. Barinov, M. Kiskinova, and A. Taleb-Ibrahimi, *Surf. Sci.* **564**, 121 (2004).
- [17] K. Eguchi, Y. Takagi, T. Nakagawa, and T. Yokoyama, *Phys. Rev. B* **85**, 174415 (2012).
- [18] K. Eguchi, Y. Takagi, T. Nakagawa, and T. Yokoyama, *J. Phys.: Conf. Ser.* **430**, 012129 (2013).
- [19] S. Gwo, C.-P. Chou, C.-L. Wu, Y.-J. Ye, S.-J. Tsai, W.-C. Lin, and M.-T. Lin, *Phys. Rev. Lett.* **90**, 185506 (2003).
- [20] R. Flammini, F. Wiame, R. Belkhou, A. Taleb-Ibrahimi, and P. Moras, *Surf. Sci.* **606**, 1215 (2012).
- [21] E. Khramtsova, A. Saranin, and V. Lifshits, *Surf. Sci.* **295**, 319 (1993).
- [22] R. Flammini, F. Wiame, R. Belkhou, A. Taleb-Ibrahimi, C. Spezzani, P. Moras, and C. Crotti, *J. Appl. Phys.* **103**, 083528 (2008).
- [23] S. Salimian, S. Xiang, S. Colonna, F. Ronci, M. Fosca, F. Rossella, F. Beltram, R. Flammini, and S. Heun, *Adv. Mater. Interfaces* **7**, 1902175 (2020).
- [24] M. A. Sobolewski and C. R. Helms, *Appl. Phys. Lett.* **54**, 638 (1989).
- [25] L. Huang, S. J. Chey, and J. H. Weaver, *Surf. Sci.* **416**, L1101 (1998).
- [26] I. Matsuda, H. W. Yeom, T. Tanikawa, K. Tono, T. Nagao, S. Hasegawa, and T. Ohta, *Phys. Rev. B* **63**, 125325 (2001).
- [27] P. Allegrini, P. Sheverdyaeva, D. Trucchi, F. Ronci, S. Colonna, P. Moras, and R. Flammini, *Appl. Surf. Sci.* **466**, 59 (2019).
- [28] Z. Zhang, Q. Niu, and C.-K. Shih, *Phys. Rev. Lett.* **80**, 5381 (1998).
- [29] G. Neuhold and K. Horn, *Phys. Rev. Lett.* **78**, 1327 (1997).
- [30] R. Losio, K. N. Altmann, and F. J. Himpsel, *Phys. Rev. B* **61**, 10845 (2000).
- [31] See Supplemental Material at <http://link.aps.org/supplemental/10.1103/PhysRevMaterials.5.084604> for raw data and data handling of photoemission intensity maps.
- [32] P. M. Sheverdyaeva, S. K. Mahatha, F. Ronci, S. Colonna, P. Moras, M. Satta, and R. Flammini, *J. Phys.: Condens. Matter* **29**, 215001 (2017).
- [33] T. C. Hsieh, P. John, T. Miller, and T.-C. Chiang, *Phys. Rev. B* **35**, 3728 (1987).
- [34] R. Heckingbottom and P. Wood, *Surf. Sci.* **36**, 594 (1973).
- [35] A. Schrott and S. Fain, *Surf. Sci.* **111**, 39 (1981).
- [36] W. Shockley, *Phys. Rev.* **56**, 317 (1939).
- [37] L. Aballe, C. Rogero, P. Kratzer, S. Gokhale, and K. Horn, *Phys. Rev. Lett.* **87**, 156801 (2001).
- [38] N. J. Speer, S.-J. Tang, T. Miller, and T.-C. Chiang, *Science* **314**, 804 (2006).
- [39] J. Davies, *The Physics of Low-Dimensional Semiconductors: An Introduction* (Cambridge University Press, Cambridge, U.K., 1997).
- [40] S.-J. Tang, L. Basile, T. Miller, and T.-C. Chiang, *Phys. Rev. Lett.* **93**, 216804 (2004).
- [41] A. Arranz, J. F. Sánchez-Royo, J. Avila, V. Pérez-Dieste, P. Dumas, and M. C. Asensio, *Phys. Rev. B* **65**, 195410 (2002).
- [42] S. Starfelt, H. M. Zhang, and L. S. O. Johansson, *Phys. Rev. B* **97**, 195430 (2018).
- [43] S. K. Mahatha and K. S. R. Menon, *J. Phys.: Condens. Matter* **25**, 115501 (2013).

- [44] P. Moras, D. Wortmann, G. Bihlmayer, L. Ferrari, G. Alejandro, P. H. Zhou, D. Topwal, P. M. Sheverdyeva, S. Blügel, and C. Carbone, *Phys. Rev. B* **82**, 155427 (2010).
- [45] C. J. Powell and A. Jablonski, *J. Phys. Chem. Ref. Data* **28**, 19 (1999).
- [46] Z. Suo and Z. Zhang, *Phys. Rev. B* **58**, 5116 (1998).
- [47] N. V. Smith, *Phys. Rev. B* **32**, 3549 (1985).
- [48] M. A. Mueller, A. Samsavar, T. Miller, and T.-C. Chiang, *Phys. Rev. B* **40**, 5845 (1989).
- [49] W. Mönch, *J. Vac. Sci. Technol. B* **14**, 2985 (1996).
- [50] H.-M. Lee, C.-T. Kuo, H.-W. Shiu, C.-H. Chen, and S. Gwo, *Appl. Phys. Lett.* **95**, 222104 (2009).
- [51] F. J. Himpsel, *J. Phys.: Condens. Matter* **11**, 9483 (1999).